Correlation of Separation Shock Motion with Pressure Fluctuations in the Incoming Boundary Layer

M. E. Erengil* and D. S. Dolling†
University of Texas at Austin, Austin, Texas 78712

Fluctuating wall pressures have been measured simultaneously in the incoming undisturbed turbulent boundary layer and under the unsteady separation shock in a Mach 5 compression ramp interaction. Conditional sampling algorithms, a variable-window ensemble averaging technique, and the variable interval time averaging technique have been used to investigate the possibility of a correlation between pressure fluctuations in the incoming flow and the separation shock wave motion. The results show only weak evidence of a correlation for large-scale downstream sweeps of the shock wave and none for large-scale upstream sweeps. In contrast, there is a distinct correlation for changes in the direction of motion of the separation shock wave. For shock turnarounds, specific pressure fluctuations (or "signatures") are convected into the interaction and are coincident with the shock foot at the time of the turnaround. The pressure signatures are different for upstream-to-downstream turnarounds and vice versa. The pressure signatures are not only evident in the ensemble averages, but also through visual inspection of individual ensembles. Thus it appears that the high-frequency jitter component of the shock motion is caused by large-scale turbulent structures that are convected into the interaction.

Introduction

EARLIER work in several different test facilities has shown that the separation shock wave in compression ramp,[1-4] flare,[5] and step-induced interactions[6] is unsteady. The unsteadiness is characterized by a relatively low-frequency, broadband motion, with a mean value of about 1 kHz. The length scale of the shock motion is of the order of the incoming turbulent boundary-layer thickness, δ_0, and extends from the upstream influence line *UI*, where the mean wall pressure $\overline{P}_w$ first rises, to the separation line *S*, obtained from surface tracer patterns. In fact, it is the occasional presence of the separation shock at these upstream stations that increases $\overline{P}_w$ above the level of the incoming undisturbed turbulent boundary layer. Because of the nature of the wall pressure signal (see Fig. 1c), the region between *UI* and *S* is called intermittent. The intermittency at any point, given by γ, is defined as the fraction of total time the separation shock is upstream of that point.

Recent work in interactions generated by compression ramps and circular cylinders has shown that separation is also intermittent.[7,8] The instantaneous separation point is just downstream of the translating shock foot, and it has been shown that the separation line indicated by surface tracer methods is not the mean value but the downstream boundary of the region of intermittent separation. In a Mach 5 compression ramp interaction,[1] it has been shown that the separation bubble "expands and contracts like a balloon," which is consistent with the earlier work of Kussoy et al.[5] in a Mach 3 cylinder-flare interaction. This unsteadiness, as discussed in Ref. 9, is probably the primary cause of the large discrepancies between computed and experimental wall pressure distributions upstream of the ramp corner.

The details of the separation shock motion in a Mach 5 compression ramp interaction have been studied by Boitnott.[10] Eight pressure transducers were placed upstream of the ramp corner as sketched in Fig. 2 and sampled simultaneously at 110 kHz/channel. From the pressure signals it could be determined which "bin" (see the inset to Fig. 2) the shock was in during each sampling interval. The bin history was used to produce a video, copies of which are available from the second author of the present paper. A typical bin history over 1 ms is shown in Fig. 2. Two superposed types of motion are evident; around t_1, for example, the shock undergoes a relatively high-frequency "jitter" as it translates back and forth between bins 2 and 3, while around t_2 it undergoes a downstream sweep from bins 6 to 2. At other times, such as around t_3, it sweeps forward (from bin 3 to 6), undergoes a "jittering" motion before sweeping back to 3. If the shock unsteadiness is ever to be modeled numerically or controlled, some physical understanding of the mechanism(s) causing the motion is needed. If it is driven by certain large-scale turbulent structures in the incoming boundary layer, or by instabilities in the separated shear layer, it is unlikely at this stage that such mechanisms can be investigated numerically. In the near term, it is more likely that the cause will be deduced from careful, focused experiments.

This is a very difficult task and, to the authors' knowledge, there have only been two experiments with this objective, both in the same Mach 3 blowdown facility, and both using compression ramps. Andreopoulos and Muck[11] reported that the mean separation shock period T_m was independent of position in the intermittent region and independent of the ramp angle α (= 16 deg, 20 deg, 24 deg). The measured shock zero-crossing frequency f_z ($\equiv 1/T_m$) was $0.13U_\infty/\delta_0$, where U_∞ is the freestream velocity and δ_0 is the incoming boundary-layer thickness. The zero-crossing frequency is simply the number of crossings per second over a given transducer by the separation shock wave. The authors claimed that this was the same order as the estimated bursting frequency in the incoming boundary layer and concluded that "the incoming boundary layer is largely responsible for the shock wave motion." From their additional observation that the measured shock speeds were the same order as velocity fluctuations in the flowfield, they also argued that this "represents further evidence that the turbulence of the incoming boundary layer is largely responsible for the shock motion."

In the absence of a direct correlation between specific turbulent motions and specific shock motions, this seems to be

Received Aug. 27, 1990; revision received April 18, 1991; accepted for publication April 18, 1991.

*Graduate Research Assistant, Department of Aerospace Engineering and Engineering Mechanics. Member AIAA.

†Associate Professor, Department of Aerospace Engineering and Engineering Mechanics. Associate Fellow AIAA.

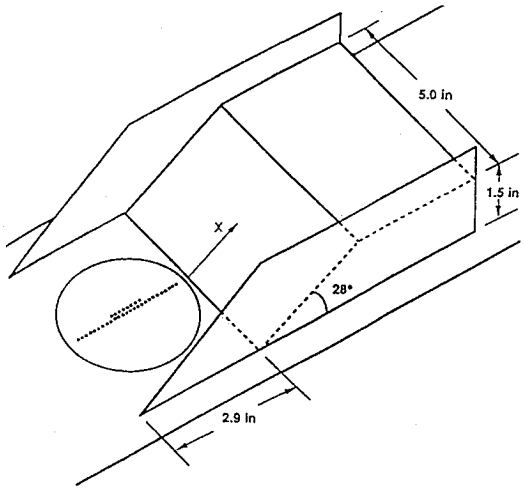

Fig. 1a Model and coordinate system.

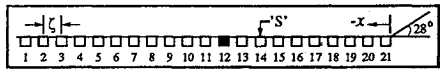

Fig. 1b Transducer positions upstream of compression corner.

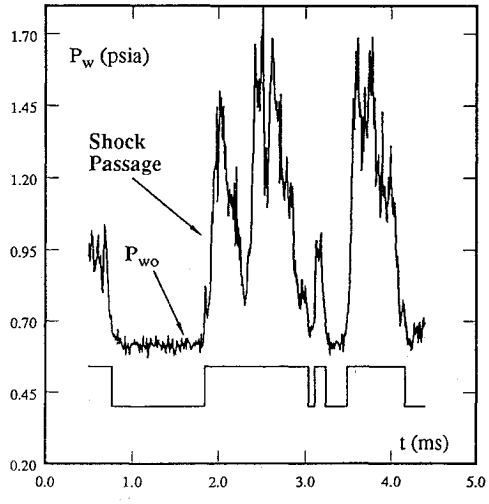

Fig. 1c Typical wall pressure signal in the intermittent region.

a premature conclusion. If the shock frequency is controlled by turbulent bursts and/or velocity fluctuations, then in a given incoming boundary layer the shock zero-crossing frequency f_z and streamwise length scale of its motion would be fixed. This is not the case.[12] For cylinder-induced interactions, in a fixed incoming boundary layer,[13] f_z decreases as the cylinder diameter D increases, and the shock motion length scale increases as D increases. Further, as shown in Ref. 12, the one-threshold algorithm used in Ref. 11 to calculate f_z probably overestimates its magnitude due to the algorithm's inability to discriminate between shock-induced pressure fluctuations and turbulent fluctuations. A more accurate two-threshold approach[12] would probably yield values of f_z of about half of those quoted in Ref. 11, i.e., $0.065U_\infty/\delta_0$.

The second experiment was by Tran and was done using the same boundary layer and a 20-deg compression ramp.[14] One transducer was placed on the upstream influence line and the other further upstream in the incoming boundary layer. The upstream channel was used as a trigger and sampling was carried out on the downstream one. Using the variable interval time averaging (VITA) technique, Tran found little correlation between events detected on the upstream channel and the shock-induced pressure pulses on the downstream channel. Close observation showed that "in many instances, the details of the pressure fluctuations of the upstream signal were preserved at the downstream station at a

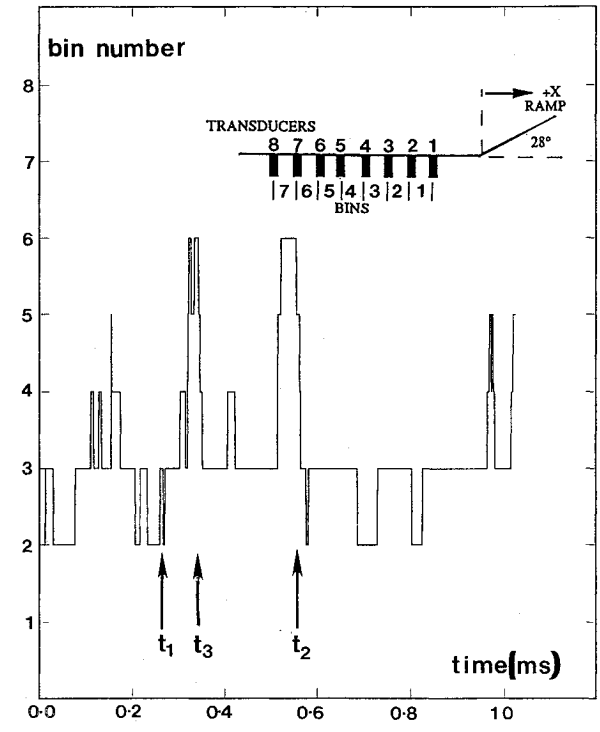

Fig. 2 Shock position as a function of time.

time delay corresponding approximately to the time that it would take for the large-scale structure to travel between the two stations." Tran concluded that the pressure pulses in the intermittent region due to the separation shock were independent of the large-scale turbulent structures that are convected into the interaction.

Tran's conclusion must also be treated with caution. Only a single transducer was placed in the intermittent region, close to its upstream edge. It is possible that the shock moved upstream and downstream in response to incoming turbulent eddies, but remained downstream of the transducer whose output was being used to calculate the ensembles. It would be better to trigger on the large pressure pulses on the downstream channel caused by the separation shock, and then ensemble average on the upstream channel in the undisturbed boundary layer. In this way, the triggering event is well defined, and ensemble averages can be more easily interpreted.

In the present study, carried out using a 28-deg compression ramp in a Mach 5 blowdown tunnel, an attempt has been made to re-examine this question. In this experiment, wall pressure fluctuations have been measured simultaneously on up to eight channels in the incoming boundary layer and in the intermittent region. In this case, specific separation shock motions over the downstream channels have been used as triggers to calculate ensemble averages on the upstream channels. In addition, individual events have been examined. The primary objective was to determine if large-scale motions of the separation shock or shock wave changes in direction (both or neither) correlated with specific types of pressure fluctuations in the incoming undisturbed turbulent boundary layer.

Experimental Program

Wind Tunnel and Model

The experiments were conducted in the Mach 5 blowdown tunnel of the University of Texas at Austin. This tunnel has a constant area test section that measures 17.78 × 15.24 cm (7 × 6 in.) in cross section and 30.48 cm (12 in.) in length. An instrumented brass plug 8.57 cm (3.375 in.) in diameter was mounted flush with the tunnel floor. This plug has a row of 26 transducer ports along its centerline and another row of 8 transducer ports parallel to and 2.92 mm (0.115 in.,

$0.17\delta_0$) from the centerline row. The spacing, ζ, between any two transducer ports is 2.92 mm (0.115 in.) center-to-center. The plug can be rotated to align the transducer ports either streamwise or spanwise. Dummy brass plugs were mounted flush in all unused transducer ports.

The model was a 28-deg unswept aluminum compression ramp, 12.70 cm (5 in.) wide and 2.81 cm (1.5 in.) high. Aerodynamic fences with sharpened leading edges were attached to both sides of the ramp to avoid spanwise spillage and to isolate the interaction from the sidewall boundary layers. The model and the coordinate system are sketched in Fig. 1a. The schematic in Fig. 1b shows the transducer ports upstream of the compression corner. The symbol '*S*' indicates the location of separation, determined from surface tracers, and the filled marker is the position at which the time history of Fig. 1c was measured. For convenience, the dimensions in the figures are given in English units.

Freestream and Boundary-Layer Flow Properties

The boundary-layer properties were determined from pitot surveys made with a probe having a tip orifice 0.20 mm (0.008 in.) high and 0.38 mm (0.015 in.) wide. The incoming turbulent boundary layer underwent natural transition well upstream of the test section. In the calculation of the velocity profile, the static pressure and the total temperature were assumed constant through the boundary layer with no heat transfer at the wall. The nominal properties of the incoming freestream flow are given in Table 1. Detailed information about the characteristics of the turbulent boundary layer can be found in Ref. 8. Table 2 lists some of the basic quantities. Standard nomenclature is used.

Instrumentation

Up to eight high-frequency response, Kulite absolute pressure transducers were used to measure the wall pressure fluctuations. They were installed flush with the surface of the instrumentation plug, which was installed flush with the funnel floor. The transducers have a nominal outer diameter of 1.59 mm (0.0625 in.) and a pressure-sensitive diaphragm 0.71 mm (0.028 in.) in diameter. Two types were used. Model XCW-062-15A, with a pressure range of 0–103 kPa (0–15 psia), has a diaphragm natural frequency of 250 kHz, and model XCQ-062-50A, with a pressure range of 0–345 kPa (0–50 psia), has a diaphragm natural frequency of 500 kHz. Perforated protective screens, which shield the diaphragm from dust particles, limit the effective frequency response of both models to about 50 kHz. The transducers were calibrated statically using a Heise digital pressure gauge (model 710A) accurate to 7 Pa (0.001 psia).

Table 1 Incoming flow conditions

M_∞	4.95	4.95
U_∞	764 m/s	2507 ft/s
Re_∞	49.6×10^6/m	15.1×10^6/ft
P_0	2.17×10^6 N/m^2	315 psia
T_0	350K	643°R

Table 2 Undisturbed boundary-layer parameters

Parameter	Tunnel Center
δ_0 (cm)	1.75
δ^* (cm)	0.64
θ ($\times 10^2$) (cm)	5.31
Π	0.30
H	12.0
Re_θ ($\times 10^{-5}$)	2.59
C_f ($\times 10^4$)	7.97

The output of each transducer was amplified by either Dynamics model 7525, Measurements Group model 2311, or PARC model 113 amplifiers, and then low-pass filtered using Itaco model 4113 or model 4213 analog filters. Amplifier gain settings were adjusted to provide maximum amplitude resolution and varied depending on the type of transducer used and its position in the interaction. The filter cutoff frequency was set at 50 kHz for sampling frequencies of 110 kHz or higher. To resolve the lower frequency content of the incoming boundary layer better, some experiments were sampled at 50 kHz and filtered at 10 kHz.

The filtered signals were digitized using a MASSCOMP 5500 data acquisition system. The data acquisition system has two 12-bit A/D converters with sample-and-hold. Each A/D converter outputs 0–4095 counts for inputs of 0–10 V (in unipolar mode) or −5–5 V (in bipolar mode). The resolution of the overall measuring system ranged from 3 Pa/count (0.0004 psia/count) for positions close to the upstream influence line to 5 Pa/count (0.0007 psia/count) close to the ramp corner. Signal-to-noise ratios were in the range 200–400 for the majority of tests.

Data Acquisition

Several sets of data were taken using strategically positioned transducers. Depending on the purpose of the experiments, sampling rates varied from 50 kHz to 500 kHz per channel. In all tests, 800 records of data were taken (1024 datapoints per record). In phase 1, tests were made in the absence of the compression ramp to characterize the undisturbed turbulent boundary layer. Several sets of simultaneous multichannel measurements were made at different sampling rates to resolve the energy content of different frequency ranges in the turbulent boundary layer. Power spectra calculated from data sampled at 50 kHz and 200 kHz are plotted in Fig. 3. The frequency resolution for the former is 48.8 Hz and that of the latter is 195 Hz. There is no evidence of any significant energy concentrations at the low frequencies (0–3 kHz) characteristic of the separation shock motion. In phase 2, transducers were placed in the intermittent region and in the incoming undisturbed flow, and multichannel measurements were made at sampling rates of 200 kHz, 250 kHz, and 500 kHz per channel. To monitor the separation shock motion, either one transducer or two transducers spaced 2.92 mm (0.115 in.) apart were held fixed in the intermittent region. The other transducer(s) were placed several spacings apart further upstream to measure the pressure fluctuations in the incoming undisturbed boundary layer.

Data from an earlier experiment[9] were also analyzed. The same model was used in the same facility under the same flow conditions, but with the transducers arranged differently than in the current experiment. Eight transducers, spaced 1ζ apart, were aligned streamwise in the intermittent region and 100 records per channel were taken at a sampling rate of 110 kHz per channel. With this configuration, the transducers almost spanned the entire intermittent region.

Interaction Properties

Distributions of the normalized mean wall pressure, $\overline{P}_w/\overline{P}_{wo}$, and the rms of the fluctuations, σ_{P_w}, are shown in Fig. 4a. $\overline{P}_{wo}$ is the mean pressure in the incoming boundary layer. The *solid line* indicated by $(P_2/P_1)_{\text{inv}}$ is the pressure ratio across the inviscid shock. Distributions of the intermittency γ (shown by *crosses*) and zero-crossing frequency f_z (shown by *circles*) are plotted in Fig. 4b. The *dashed line* represents an error function fit to the intermittency curve. The schematic on top of Fig. 4b shows the transducer positions upstream of the compression corner. Again, for convenience, the dimensions in the figures are given in English units. The calculation methods are described in Ref. 12. These results were presented and discussed in an earlier paper[2] and the reader is referred to it for details. They are shown here as proof that

this particular interaction has the usual features of nominally two-dimensional separated compression ramp interactions.

Analysis Techniques

Two types of analyses have been carried out. 1) Using particular types of shock motions as a trigger, ensemble-averaged pressure histories were calculated for each channel over a short time span beginning just before the triggering event and terminating shortly after. The objective was to determine if the particular shock motion (i.e., the triggering event) correlates with the convection into the interaction of particular pressure fluctuations having specific "signatures," or with any other pressure variations in the incoming flow. 2) Using the triggering techniques above (i.e., the same events), individual ensembles were extracted from each channel and examined visually and by using the VITA technique. The objective was to determine if any characteristic "signatures" seen in the ensemble averages could also be clearly observed in single events.

The triggering events are determined using box-car representations of the intermittent pressure signals. A two-threshold method was used to detect separation shock passages and to convert the intermittent pressure signals into boxcars. This technique is described in detail in an earlier paper by Dolling and Brusniak.[12] In the boxcar representation, shock crossings in the upstream and downstream directions are characterized by rise and fall times, respectively. To determine the shock fall times more accurately, a third threshold was introduced. The reason why this is necessary and how the method works is described in Ref. 2. The ensemble-averaging method employs a variable-width window and is also described in detail in Ref. 2. The remainder of this section focuses on the triggering techniques used, since this is critical to the interpretation and understanding of the results.

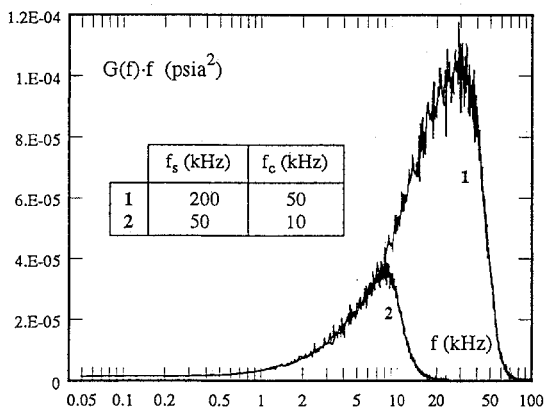

Fig. 3 Power spectral densities in the incoming undisturbed boundary layer.

Triggering Techniques

Four types of separation shock motions were used as triggers. They were: 1) a continuous upstream sweep of the separation shock (referred to as *us*-motion), 2) a continuous downstream sweep of the separation shock (*ds*-motion), 3) shock motion change of direction from upstream to downstream (*ud*-motion), and 4) shock motion change of direction from downstream to upstream (*du*-motion). The application of each triggering technique is described below with the aid of nested boxcar functions and shock trajectories shown in Figs. 5a through 5d. These techniques are described for N adjacent transducers in the intermittent region, where $N \geq 3$. In cases where $N < 3$, *ud*- and *du*-motions can still be detected; however, *us*- and *ds*-motions are not well-defined events, and should not be used as triggering events. Also, note that the maximum number of adjacent transducers needed for detection of *ud*- and *du*-motions is 3, whereas there is not a limit on the maximum number of transducers that can be used in the detection of *us*- and *ds*-motions.

us-motion as a Trigger

A *us*-motion is an upstream sweep of the separation shock over N transducers. Fig. 5a shows the schematic representation of such a motion, the corresponding nested boxcars, and shock trajectories for $N = 3$. In this representation, a *us*-motion over N transducers corresponds to N consecutive rises in the nested boxcars. For such an event, the data points from the rise time of the downstream channel ($n = 6$) to the rise time of the upstream channel ($n = 4$) are extracted from each channel to form one ensemble block, W, for each channel. The time $\tau = 0$ is assigned to the rise time of the shock passage over the intermediate channel ($n = 5$) or one of the intermediate channels if $N > 3$. Similarly, the next occurrence of N consecutive rises will define the next ensemble for this particular motion. The ensembles for respective channels are then added and averaged to from the ensemble-averaged pressure histories for each channel. As N increases, the number of events decreases rapidly, since the spatial sweep is larger and these are rarer events. Also, a sweep is clearly affected

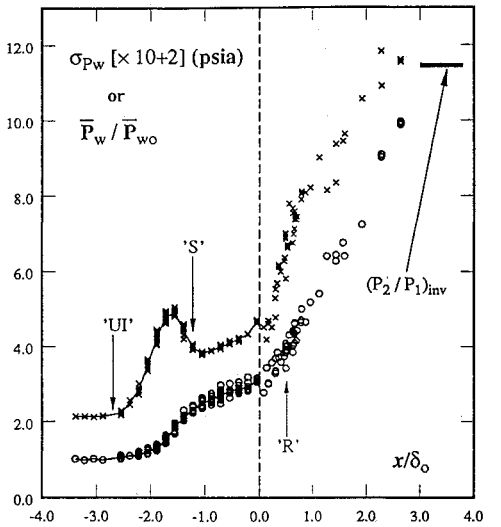

Fig. 4a Standard deviation and normalized mean pressure distributions.

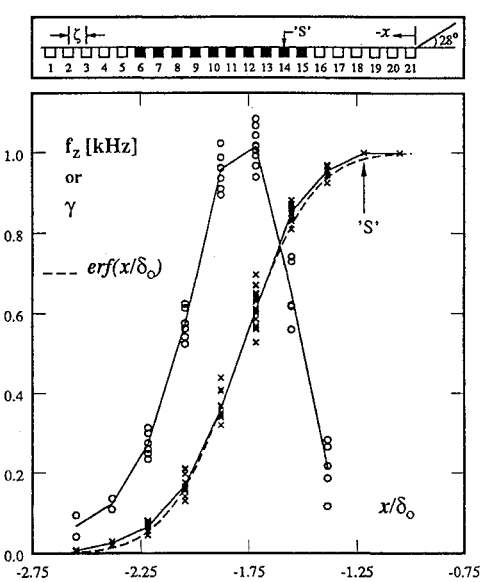

Fig. 4b Intermittency and zero-crossing frequency distributions.

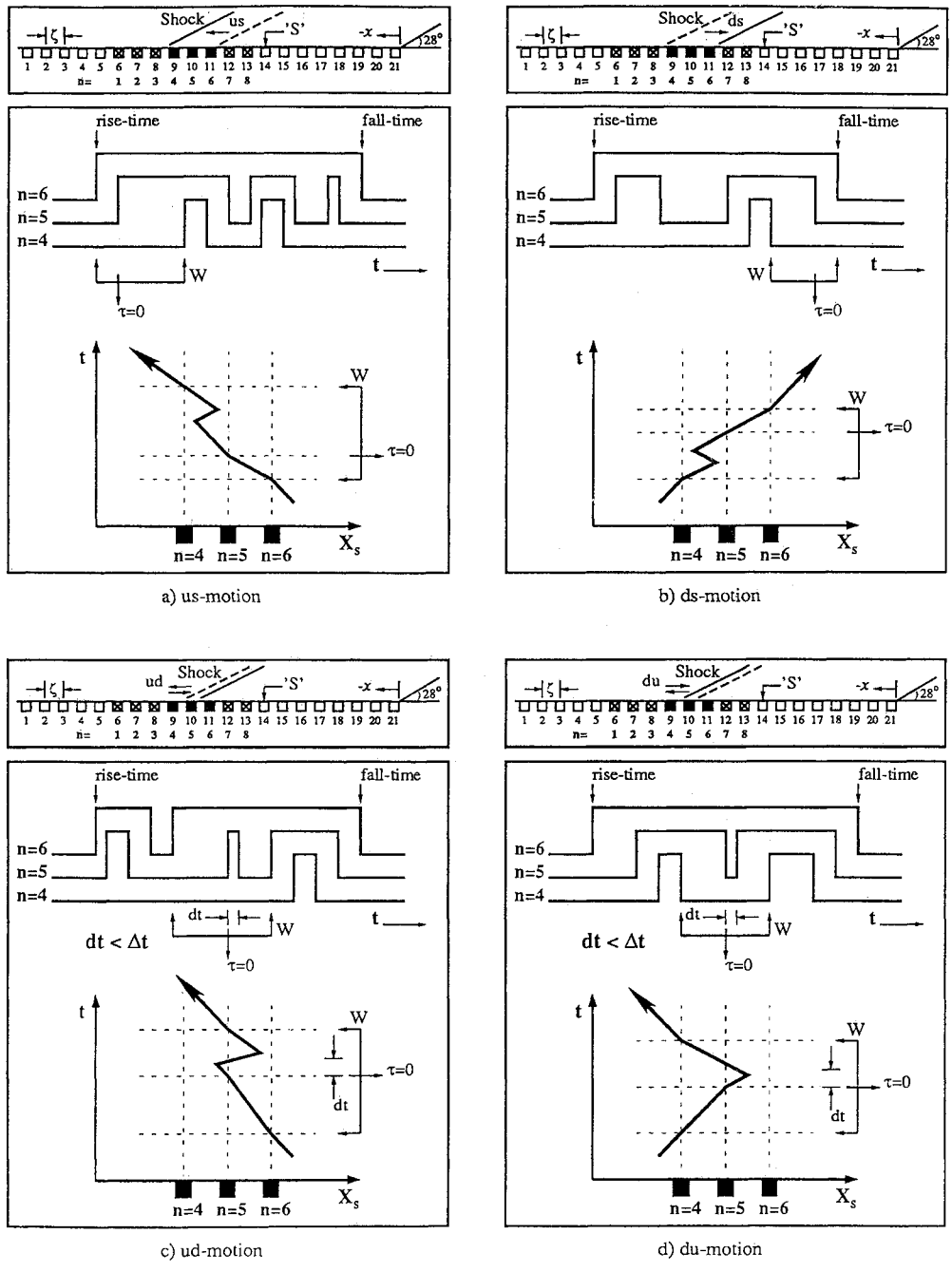

Fig. 5 Triggering techniques.

by spatial resolution problems. If an even number of turnarounds occur during the *us*-motion, but take place in between transducers, they will not be detected. An example of such an occurrence between channels 4 and 5 is shown in the shock trajectory of Fig. 5a. Hence, the ensembles for the *us*-motion may well include some even number of turnarounds which cannot be detected given the spatial resolution of the experiments. Consequently, the ensemble-averaged histories for the *us*-motion must be interpreted with caution.

ds-motion as a Trigger

A *ds*-motion is a sweep of the separation shock in the downstream direction over N transducers. Fig. 5b shows the schematic representation of such a motion, the corresponding nested boxcars, and shock trajectory for $N = 3$. In this case, there are N consecutive falls and the data block for each ensemble is from the fall time of the upstream channel ($n = 4$) to the fall time of the downstream channel ($n = 6$). Again, the time $\tau = 0$ is taken as the fall time of the shock passage over the intermediate channel ($n = 5$), and the process is repeated for the next occurrence of N consecutive falls. The comments about spatial resolution made above also apply to the *ds*-motion. A possible double turnaround occurring between transducers 4 and 5 is also sketched in the shock trajectory; however, it cannot be detected due to the spatial resolution problems.

ud-motion as a Trigger

A *ud*-motion is a change of direction (or turnaround) from upstream to downstream direction of motion within a user-specified time span Δt. Fig. 5c shows the schematic representation, the corresponding nested boxcars, and shock trajectory for $N = 3$. In the nested boxcar representation, a turnaround from upstream to downstream occurs when the difference between the fall and rise times of shock crossings over the intermediate transducer, dt, is less than the specified turnaround time Δt. In this case, the upstream ($n = 4$) and down-

stream ($n = 6$) transducers are used to ensure that the separation shock is bracketed between these two transducers during the *ud* motion. This ensures that the ensembles taken from the upstream ($n = 1$, 2, or 3) or downstream ($n = 7$ or 8) channels are not affected by shock-induced pressure fluctuations. Once a *ud*-motion is detected, the ensemble window is determined as follows. The fall time of the previous shock crossing over the intermediate channel ($n = 5$) and the rise time of the following shock crossing are used as first guesses to define the data block width for the ensemble. If the rise time of the downstream channel ($n = 6$) is greater than the fall time of the previous shock crossing over transducer 5 (i.e., the first guess), this indicates that the separation shock was downstream of the downstream transducer ($n = 6$) for part of the data block. For such cases, the rise time of the shock crossing over the downstream transducer ($n = 6$) is taken as the lower limit of the data block (instead of the first guess) to ensure that the separation shock stayed upstream of the downstream transducer ($n = 6$) during the ensemble block. Similarly, if the fall time of the downstream channel ($n = 6$) is less than the rise time of the following shock crossing over transducer 5 (i.e., the first guess), then this time is used as the upper limit of the data block (instead of the first guess) to ensure that the separation shock stays upstream of the downstream transducer ($n = 6$) for the duration of each ensemble. That the separation shock stays downstream of the upstream channel ($n = 4$) is ascertained by making sure that there were no rise or fall times on the upstream channel during the *ud*-motion (i.e., within the ensemble block W. Once the ensemble block is determined, the $\tau = 0$ value is then assigned to the rise time of the shock crossing over the intermediate channel ($n = 5$).

du-motion as a Trigger

A *du*-motion is a change of direction of shock motion from downstream to upstream within a user specified time span Δt. Fig. 5d shows the schematic representation, the corresponding nested boxcars, and shock trajectory for $N = 3$. Again, the upstream ($n = 4$) and downstream ($n = 6$) transducers are used to ensure that the separation shock is bracketed between them during the *du*-motion. As can be seen in the nested boxcar representation, a *du*-motion occurs when the time span between fall and rise times of the shock crossing over the intermediate transducer ($n = 5$) is less than the specified Δt. Once a *du*-motion is detected, it is then necessary to define the beginning and the end of the ensemble block. In this case, the rise time of the previous shock crossing over the intermediate transducer ($n = 5$) is taken as the beginning of the ensemble block unless there exists a fall time of a shock crossing over the upstream transducer ($n = 4$) that is greater than this rise time, then the fall time of this shock crossing over the upstream transducer ($n = 4$) is taken as the beginning of the ensemble block W. This procedure ensures that the separation shock remains downstream of the upstream transducer ($n = 4$). Similarly, the end of the ensemble block is taken as the fall time of the following shock crossing over the intermediate transducer ($n = 5$), unless there exists a rise time of a shock crossing over the upstream transducer ($n = 4$) that is less than this fall time, then the rise-time of this shock crossing over the upstream transducer ($n = 4$) is taken as the end of the ensemble block W. Again, this ensures that the separation shock remains downstream of the upstream transducer ($n = 4$) during the ensemble window. That the separation shock remained upstream of the downstream transducer ($n = 6$) is ensured by searching for a *du*-motion within the rise and fall times of two consecutive shock crossings over the downstream transducer ($n = 6$). Once the ensemble window is defined, the $\tau = 0$ value (or the "center" of the window) is assigned to the fall time of the shock crossing over the intermediate transducer, and the respective ensemble blocks are extracted from each channel. This procedure is repeated when the next *du*-motion is detected, and the ensemble blocks are added to form the ensemble-averaged pressure histories for each channel.

Examination of Individual Events

As mentioned earlier, individual ensembles determined using the triggering techniques above were extracted from each channel and examined further through visual inspection and the VITA technique. The objective was to determine if the individual ensembles extracted from the incoming undisturbed turbulent boundary-layer signal were consistent with the ensemble-averaged result.

The VITA technique, developed by Blackwelder and Kaplan,[15] involves calculation of the short-term variance, STV, of the signal using a suitable width moving window. A threshold level is then set to detect the passage of highly energetic fluctuations (i.e., high levels of STV). The short-term variance of the fluctuating pressure signal is defined as follows:

$$STV(x,T_0,t) = \frac{1}{T_0}\int_{t-(T0/2)}^{t+(T0/2)} [P_w(x,s)]^2\, ds - \left[\frac{1}{T_0}\int_{t-(T0/2)}^{t+(T0/2)} P_w(x,s)\, ds\right]^2$$

where T_0 is the window width over which the STV is calculated, P_w is the fluctuating wall pressure signal, t is the time, x is the spatial coordinate, and s is just a dummy variable. It should be noted that T_0 acts as a bandpass filter in this formulation. As T_0 increases, the VITA technique becomes more receptive to lower frequency fluctuations in the signal and vice versa.

The window width T_0 was chosen based on the results of the ensemble-averaged pressure histories in the incoming undisturbed turbulent boundary layer, and varied from about 55 to 65 μs. The explanation for this choice of T_0 will be given later when the results are discussed. Since the VITA technique was not used as a detection scheme to extract events for ensemble averaging, but for visual inspection purposes only, no threshold was used.

Results

Ensemble-averaged pressure histories triggered by shock sweeps (i.e., *us*- and *ds*-motions) and those triggered by shock turn-arounds (i.e., *ud*- and *du*-motions) are presented in the first and second sections below, respectively. The results for individual ensembles and from the VITA analysis are presented in the final section. Unless otherwise stated, the results are calculated using the eight-channel data of Ref. 9. Even though the sampling frequency of this data set (110 kHz) does not provide as good a time resolution as the four- or two-channel data, the large number of simultaneously sampled channels is especially helpful in the interpretation of the results. Similar results were obtained for data at the higher sampling rates.

Shock Sweeps

Figure 6 shows ensemble-averaged pressure histories calculated from 149 ensembles at eight stations in the intermittent region for the case of a *us*-motion over three transducers. At the top of the figure, the schematic shows the transducer positions upstream of the compression corner indicated by *crosses*. *Filled markers* indicate the positions of the triggering transducers (i.e. channels 4, 5, and 6) which in this case are at intermittencies of about 20, 40, and 65%, respectively. For all these sweeps, the separation shock is never upstream of the upstream triggering channel ($n = 4$). This can be verified by either examining the ensemble-averaged pressure levels on channel, $n = 3$, or by referring back to the explanation of this particular shock motion as a trigger. Given this, it is

clear that channels 1–3 measure the pressure fluctuations in the incoming undisturbed turbulent boundary layer when channels 4–6 are used as the triggering transducers. The ensemble-averaged pressure histories for these three channels show no correlation between the upstream sweep of the separation shock over the three downstream transducers (4–6) and pressure fluctuations in the incoming flow. There is no evidence of any "disturbance" or a specific pressure "signature" entering the interaction during the upstream sweep of the shock. There is also no obvious evidence of lower or higher pressure levels in the incoming undisturbed turbulent boundary layer during this motion (i.e., $\overline{P}$ on the upstream channels at $\tau = 0$ is neither high or low compared to the overall mean boundary layer pressure value for the respective channels). The same results were obtained for different positions of the triggering transducers in the intermittent region.

The corresponding ensemble-averaged pressure histories on the eight channels for a downstream sweep are shown in Fig. 7. The same three channels (i.e., 4–6) act as triggers, and ensemble-averaged pressure histories under the incoming boundary layer during the sweep are shown on channels 1–3. In this case, ensemble-averaged results were calculated from 161 ensembles. In contrast to the upstream sweep there appears to be a weak correlation between this sweep motion and activity in the boundary layer. During the sweep, around $\tau = 0$, the pressure in the incoming flow is falling. The decrease is small, at most 0.01 psia, or about one standard deviation of the undisturbed boundary-layer signal, but stands out from the background signal. The latter, given sufficient ensembles, and assuming no correlation with the shock motion would be flat and equal to the mean of the undisturbed boundary-layer signal. The downstream convection of the structure, or disturbance, causing the pressure decrease, is also evident by noting how the peak (or trough) moves toward $\tau = 0$ from channel 1 to 2 to 3.

Shock Turnarounds

Figure 8 shows the ensemble-averaged pressure histories at eight stations in the intermittent region for a shock turnaround from upstream to downstream. Again, the schematic at the top of the figure shows the transducer positions upstream of the compression corner. The transducer over which the shock turnaround occurs (i.e., the intermediate trigger, $n = 5$) is at an intermittency of about 40%. The turnaround time Δt was set at about 90 μs. Using this criterion, 350 *ud*-motions were detected at this station. The number of ensembles (i.e., the number of triggering events) is a function of the position of the triggering transducer and the turnaround time Δt. Recall that shock turnarounds are detected using the intermediate trigger. Upstream ($n = 4$) and downstream ($n = 6$) triggers are used to ensure that the separation shock remains downstream of the upstream transducer ($n = 4$) and upstream of the downstream one ($n = 6$) during the turnaround. In this case, all transducers upstream of the triggering transducer

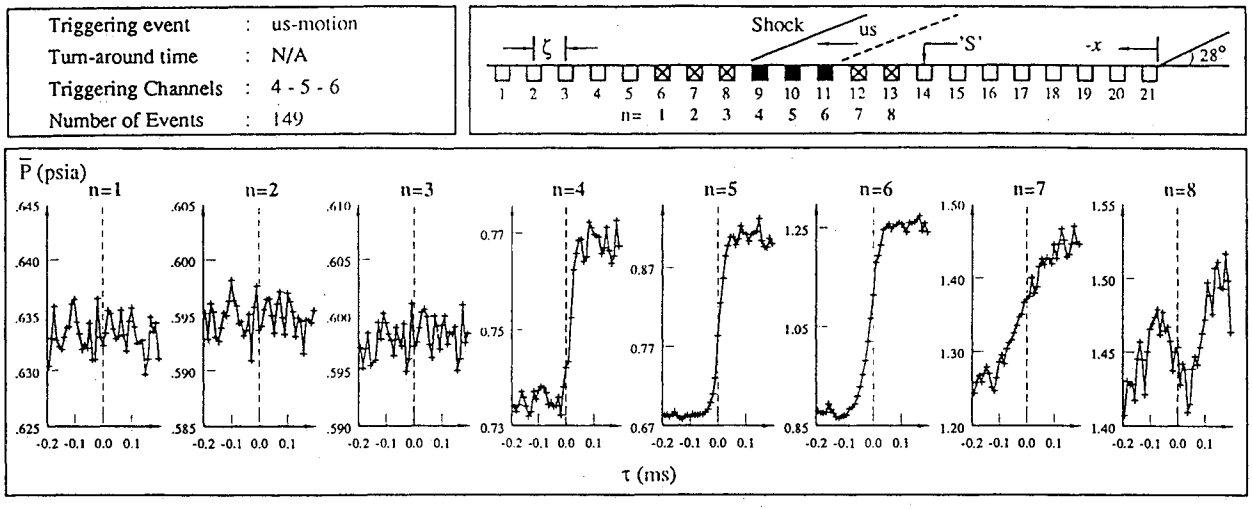

Fig. 6 Ensemble-averaged pressure histories for *us*-motion.

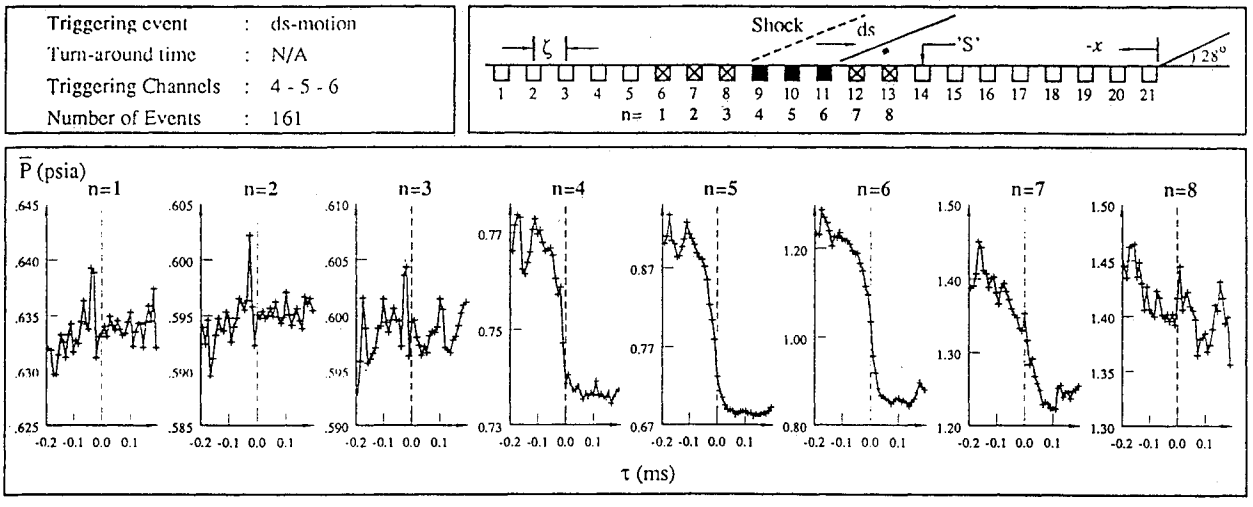

Fig. 7 Ensemble-averaged pressure histories for *ds*-motion.

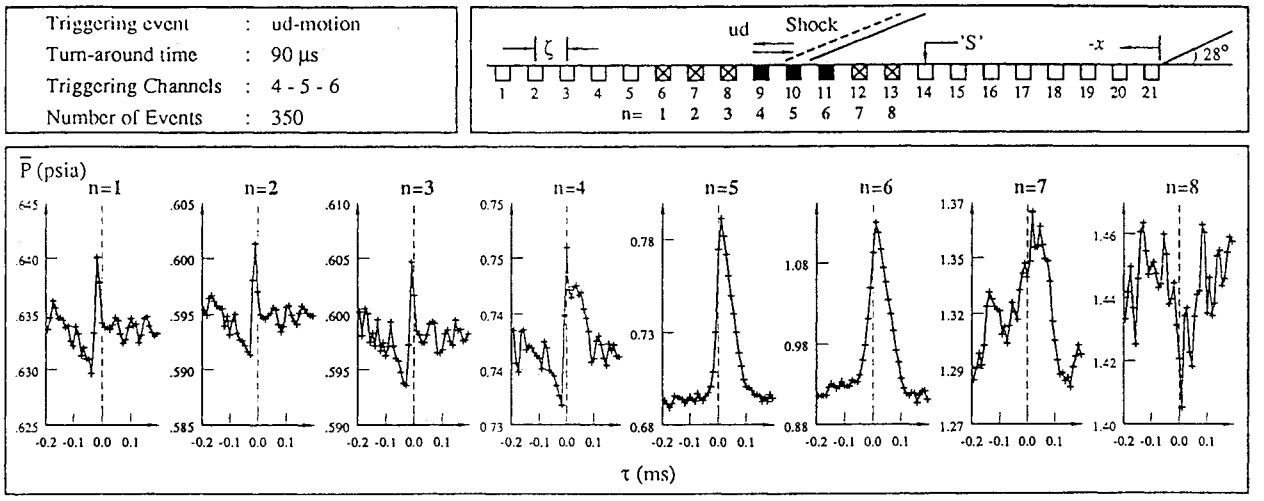

Fig. 8 Ensemble-averaged pressure histories for *ud*-motion.

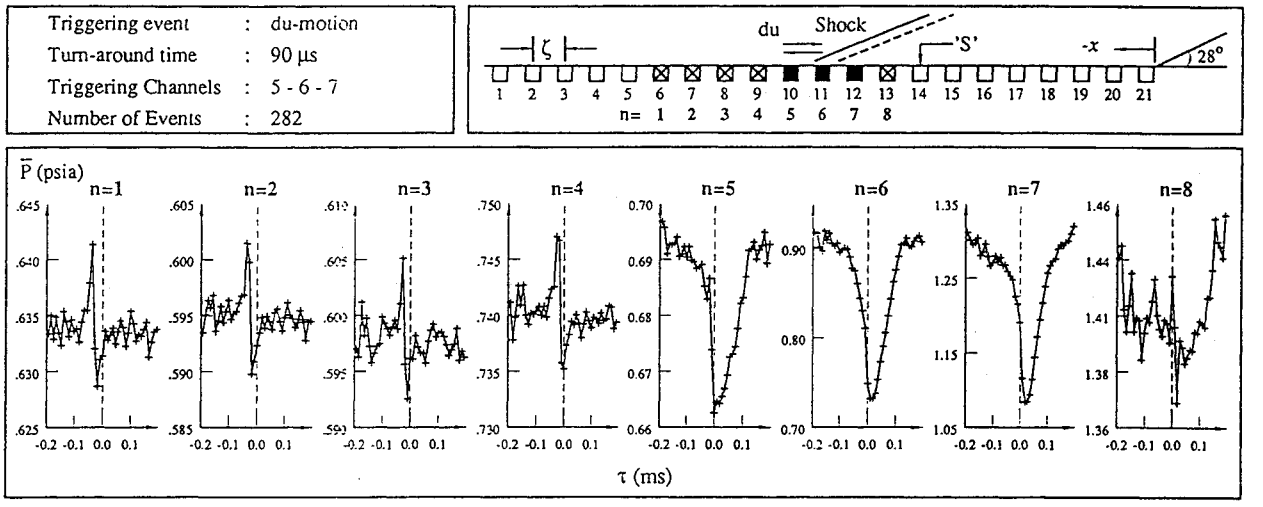

Fig. 9 Ensemble-averaged pressure histories for *du*-motion.

($n = 5$) are in the incoming undisturbed turbulent boundary layer. Ensemble-averaged pressure histories show quite clearly a distinct correlation between the pressure fluctuations in the incoming turbulent boundary layer and separation shock change of direction of motion.

By examining the ensembles on channels 1, 2, 3, and 4 it can be seen that just before $\tau = 0$ there is a pressure fall followed by a sharp rise and a fall. It is possible that this signature is generated by the passage of a turbulent structure. Its convection into the interaction is clearly evident as it transverses channels 1, 2, etc. At $\tau = 0$, as the shock turns around, the shock and the incoming pressure signature are essentially coincident. Using the maximum or minimum pressure as a reference point, estimates were made of the times required to travel one to five transducer spacings. The average convection velocity was about 0.75 U_∞ which is consistent with the broadband convection velocity calculated from cross-correlations in the undisturbed boundary layer. The time from the initial pressure fall to the return to the original pressure at the end of the signature is of order 80–100 μs. At a convection speed of 0.75 U_∞ this corresponds to a streamwise length scale of about 4.5–5.5 cm, about 2.5–3 δ_0. The same results were obtained using different transducers in the intermittent region as triggers. The only difference was the number of events detected.

Figure 9 shows the ensemble-averaged pressure histories at eight stations in the intermittent region for shock turnaround from downstream to upstream direction of motion (i.e., *du*-motion). Again, the positions of the pressure transducers as well as the triggering channels are indicated in the schematic at the top of the figure. In this case, the triggering transducer ($n = 6$) is at an intermittency of about 65%. The turnaround time Δt is the same as in the previous case (90 μs). The triggering transducer was changed from the previous case to maximize the number of events which was 282. As can be seen in the ensemble-averaged pressure histories, there is again a strong correlation between specific pressure variations in the incoming turbulent boundary layer and separation shock change of direction of motion from downstream to upstream. In this case, the ensemble-averaged pressure signatures have the opposite shape of the characteristic signatures observed for shock change of direction from upstream to downstream. These signatures, which may be due to turbulent structures, have the same length scale and convection velocities as those observed for *ud*-motion. The correlation is observed independent of the separation shock position in the intermittent region.

Examination of Individual Events

As mentioned earlier, individual events were extracted from each channel and examined visually and by the VITA technique. The data used were from the four channel experiments in which the sampling rate was 200 kHz/channel. Thus, the time resolution is superior to that in the earlier figures. Several

hundred events were examined. Figures 10a and 10b show the individual ensembles at four stations in the intermittent region, and their respective short-term variances (STVs) for a single *ud*-motion. In this example, the window width T_0 and the turnaround time Δt were 55 and 75 μs, respectively. The value of T_0 was selected by examining the ensemble-averaged pressure histories calculated from 296 ensembles for this particular case.

Considering first the unprocessed pressure ensembles in Fig. 10a, the rapid rise and fall of the shock turning around over channel 3 is evident. The convection of this pressure signature over channel 1 (2ζ further upstream in the undisturbed boundary layer) and then, 5–10 μs later, over channel 2 (1ζ further downstream) is also evident. Note that around $\tau = 0$, the pressure on channels 1 and 2 is rising, consistent with the ensemble-averaged signature (Fig. 8) for this type of motion.

For a well-defined *ud*-motion such as this, the rise and fall in pressure caused by the shock turnaround appear as two sharp peaks in the corresponding STV history (channel 3, Fig. 10b). The STV histories on channels 1 and 2 show the presence of energetic pressure fluctuations around $\tau = 0$. Examination of many STV histories shows quite clearly the presence of these energetic pressure fluctuations over the two upstream channels. However, the sequential timing information is lost since the technique averages over the window width T_0. Thus, although the presence of these fluctuations is more evident in the STV histories, their motion is more readily observed in the individual ensemble histories.

In summary, careful examination shows that well-defined individual shock turnarounds correlate with specific individual pressure signatures in the incoming flow and the structures that may be responsible for generating the signatures can be observed in the STV histories. Shock turnarounds that are not as well defined, due either to a smaller pressure rise (corresponding to cases where the shock does not fully cross the transducer before turning around), or particularly noisy or turbulent cases, do not present as clear a picture. Nevertheless, in almost all cases, the slopes of the individual pressure ensembles are positive around $\tau = 0$, as is the ensemble-averaged result. Conversely, the majority of shock turnarounds in the opposite direction (*du*-motions) have negative slopes around $\tau = 0$ on the upstream channels, which is again consistent with the ensemble-averaged results in Fig. 9.

Discussion and Summary

The results show a correlation between pressure variations in the incoming boundary layer and certain separation shock motions. For shock turnarounds, specific pressure fluctuations (or signatures) enter the interaction and are coincident with the shock foot at the time of the turnaround. For the downstream-to-upstream shock turnarounds, the characteristic pressure signature is a rise-fall-rise sequence. Conversely, for a turnaround from upstream-to-downstream the pressure signature is a fall-rise-fall sequence. Both signatures are not only evident in the ensemble averages, but also from inspection of individual events. The situation with continuous sweeps is not as clear. For upstream sweeps, there is no evidence of any characteristic pressure variation in the incoming boundary layer, whereas for downstream sweeps there is some indication that the upstream pressure falls slightly during the sweep.

Since essentially the same trigger detection scheme is used for upstream and downstream sweeps, and exactly the same data records are examined, it seems unlikely that there is some deficiency in the method which masks the existence of specific signatures in the sweep cases. It should be noted, as mentioned earlier, that sweep events are not as well defined as turnarounds. Because there is a gap between adjacent transducers, it is highly probable that the shock undergoes turnarounds within the gap during the sweep. If the turnarounds happen over a transducer, they are detectable and the en-

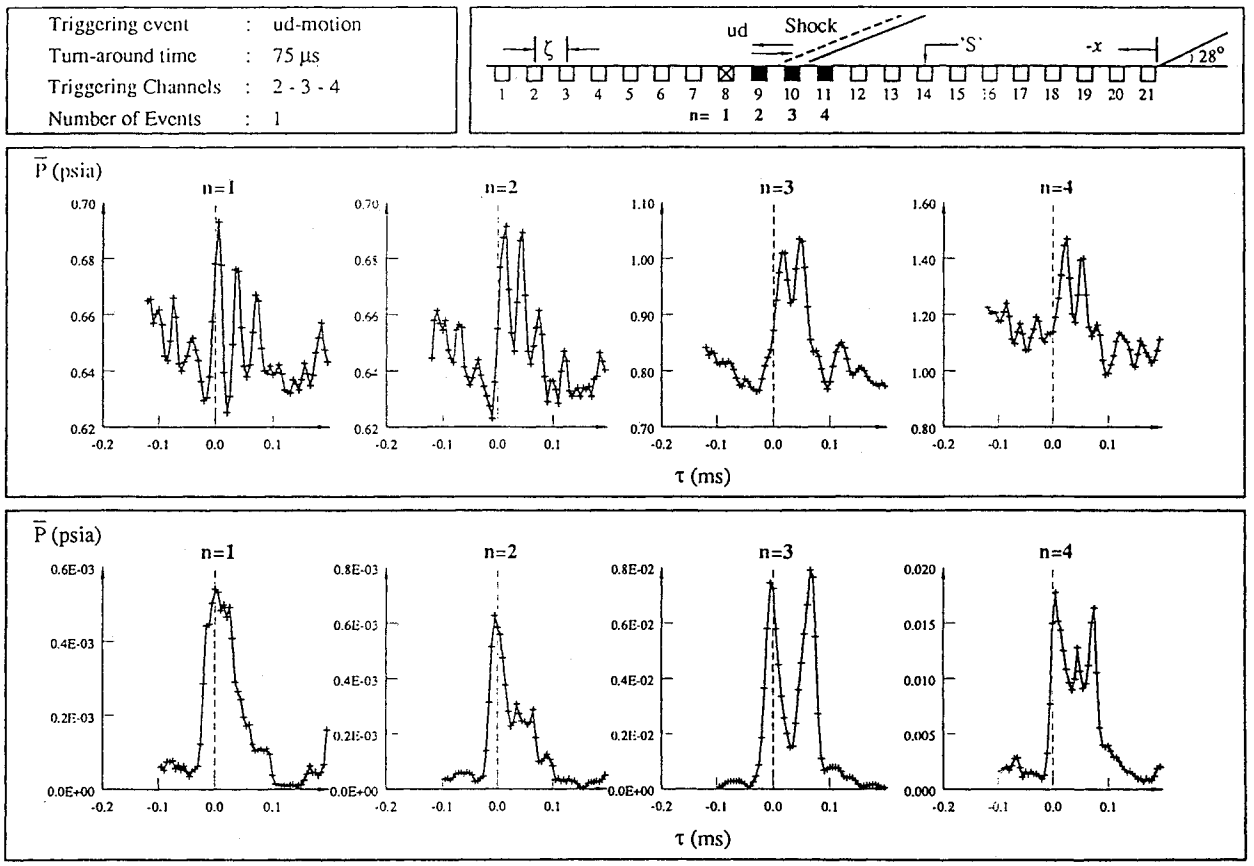

Fig. 10 a) Individual ensemble pressure histories for *ud*-motion; b) corresponding individual STV histories for *ud*-motion.

semble is rejected, but if they occur undetected between them, the ensemble is included in the averaging. Equal numbers of undetected turnarounds of opposite type could mask the characteristic signature. In contrast, for a shock turnaround the detection scheme ensures that the turnaround occurs over one transducer and the final ensemble average is only made up of one event type, namely the turnaround. The weaker correlation seen in the downstream sweep is, at least, consistent with the turnaround result. Since a downstream sweep must terminate in a downstream-to-upstream turnaround, the pressure variation for part of the time in the incoming flow for a sweep would have similar behavior to the turnaround. Comparison of Figs. 7 and 9 shows this is the case.

To the authors' knowledge, these are the first results to show a direct correlation between pressure fluctuations in the incoming flow and certain types of separation shock wave motion. It appears that the high-frequency jitter that causes the shock foot to undergo a rapid series of changes of direction of motion, or that causes it to change direction during a sweep and then continue in the same direction, is caused by the passage of specific large-scale structures. Whether the large-scale sweeps are driven by the same mechanism is not clear. The duration of such sweeps would require incoming structures whose streamwise length scale was extremely large. It seems more likely that they are affected by some larger scale, lower frequency instability or flow structure associated with the separated bubble. The evidence suggests that two mechanisms may operate simultaneously: one responsible for the large-scale sweeps, the other for the jitter. The cause of the latter appears to have been identified in the current study, whereas the cause of the former remains uncertain. New experiments in which the shock and bubble dynamics are monintored simultaneously both at the wall and in the flowfield are needed to provide an answer to this question.

Acknowledgment

The support of the Air Force Office of Scientific Research under Grant 86-0112, monitored by L. Sakell, is gratefully acknowledged.

References

[1]Gramann, R. A., and Dolling, D. S, "Dynamics of Separation and Reattachment in a Mach 5 Unswept Compression Ramp Flow," AIAA Paper 90-0380, Reno, NV, Jan. 1990.

[2]Erengil, M. E., and Dolling, D. S., "Unsteady Wave Structure near Separation in a Mach 5 Compression Ramp Interaction," *AIAA Journal*, Vol. 29, No. 5, 1991, pp. 728–735.

[3]Dolling, D. S., and Murphy, M. T., "Unsteadiness of the Separation Shock Wave in a Supersonic Compression Ramp Flowfield," *AIAA Journal*, Vol. 21, No. 12, 1983, pp. 1628–1634.

[4]Muck, K. C., Dussauge, J. P., and Bogdonoff, S. M., "Structure of the Wall Pressure Fluctuations in a Shock-Induced Separated Turbulent Flow," AIAA Paper 85-0179, Reno, NV, Jan. 1985.

[5]Kussoy, M. I., Brown, J. D., Brown, J. L., Lockman, W. K., and Horstman, C. C., "Fluctuations and Massive Separation in Three-Dimensional Shock-Wave/Boundary-Layer Interactions," 2nd International Symposium on Transport Phenomena in "Turbulent Flows," Tokyo, Japan, Oct. 25–29, 1987.

[6]Kistler, A. L., "Fluctuating Wall Pressure Under Separated Supersonic Flow," *Journal of Acoustical Society of America*, Vol. 36, March 1964, pp. 543–550.

[7]Gramann, R. A., and Dolling, D. S., "Detection of Turbulent Boundary Layer Separation Using Fluctuating Wall Pressure Signals," *AIAA Journal*, Vol. 28, No. 6, 1990, pp. 1052–1056.

[8]Gramann, R. A., "Dynamics of Separation and Reattachment in a Mach 5 Unswept Compression Ramp Flow," Ph.D. Dissertation, Dept. Aerospace Engineering and Engineering Mechanics, Univ. of Texas, Austin, TX, Dec. 1989.

[9]Marshall, T. A., and Dolling, D. S., "Spanwise Properties of the Unsteady Separation Shock in a Mach 5 Unswept Compression Ramp Interaction," AIAA Paper 90-0377, Reno, NV, Jan. 1990.

[10]Boitnott, T., "Video Visualization of Separation Shock Motion from Measured Wall Pressure Signals in Mach 5 Compression Ramp Interaction," AIAA Paper 90-0074, Reno, NV, Jan. 1990.

[11]Andreopoulos, J., and Muck, K. C., "Some New Aspects of the Shock-Wave/Boundary-Layer Interaction in Compression Ramp Flows," *Journal of Fluid Mechanics*, Vol. 180, 1987, pp. 405–428.

[12]Dolling, D. S., and Brusniak, L., "Separation Shock Motion in Fin, Cylinder, and Compression Ramp-Induced Turbulent Interactions," *AIAA Journal*, Vol. 27, No. 6, 1989, pp. 734–742.

[13]Dolling, D. S., and Smith, D. R., "Separation Shock Dynamics in Mach 5 Turbulent Interaction Induced by Cylinders," *AIAA Journal*, Vol. 27, No. 12, 1989, pp. 1698–1706.

[14]Tran, T. T., "An Experimental Investigation of Unsteadiness in Swept Shock Wave/Turbulent Boundary Layer Interactions," Ph.D. Dissertation, Mechanical and Aerospace Engineering Dept., Princeton Univ., Princeton, NJ, Oct. 1986.

[15]Blackwelder, R., and Kaplan, R. E., "On the Wall Structure of the Turbulent Boundary Layer," *Journal of Fluid Mechanics*, Vol. 76, 1976, p. 89.